HHS Public Access

Author manuscript

J Orthop Res. Author manuscript; available in PMC 2016 March 01.

Published in final edited form as:

J Orthop Res. 2015 March ; 33(3): 334–342. doi:10.1002/jor.22761.

Long-Term Loss of Osteoclasts and Unopposed Cortical Mineral Apposition Following Limited Field Irradiation

Megan E. Oest, Ph.D.[1], **Veerle Franken**[1], **Timothy Kuchera**[1], **Judy Strauss**[1], and **Timothy A. Damron, M.D.**[1]

[1]Department of Orthopedic Surgery, Upstate Medical University, Syracuse, New York

Abstract

Late-onset fragility fractures are a common complication following radiotherapy for metastatic disease and soft tissue sarcomas. Using a murine hindlimb focal irradiation model (RTx), we quantified time-dependent changes in osteoclasts and mineral apposition rate (MAR). Mice received either a single, unilateral 5 Gy exposure or four fractionated doses (4x5 Gy). Osteoclast numbers and MAR were evaluated histologically at 1, 2, 4, 8, 12, and 26 weeks post-RTx. Radiation induced an early, transient increase in osteoclasts followed by long-term depletion. Increased osteoclast numbers correlated temporally with trabecular resorption; the resorbed trabeculae were not later restored. Radiotherapy did not attenuate MAR at any time point. A transient, early increase in MAR was noted in both RTx groups, however, the 4x5 Gy group exhibited an unexpected spike in MAR eight weeks. Persistent depletion of osteoclasts permitted anabolic activity to continue unopposed, resulting in cortical thickening. These biological responses likely contribute to post-radiotherapy bone fragility via microdamage accumulation and matrix embrittlement in the absence of osteoclastic remodeling, and trabecular resorption-induced decrease in bone strength. The temporal distribution of osteoclast numbers suggests that anti-resorptive therapies may be of clinical benefit only if started prior to radiotherapy and continued through the following period of increased osteoclastic remodeling.

Keywords

radiation; osteoclast; mineral apposition; bone morphology; fracture

INTRODUCTION

Post-radiotherapy fragility fractures are a frequent complication in cancer survivors.[1; 2] Radiation is effective in soft tissue sarcoma and carcinoma treatment, but underlying bone damage is common. Overall post-radiotherapy fracture rates may reach 20% in breast cancer and soft tissue sarcoma survivors.[3; 4] Pelvic fracture rates range from is 9.5–20% (cervical and anorectal cancers), while rib fracture rates (lung cancer) range from 8–21% depending on dose.[1; 3; 5–7] Femoral fracture incidence of ~7% has also been reported.[8; 9] Clinical

Correspondence: Megan E. Oest, Department of Orthopedic Surgery, SUNY Upstate Medical University, 750 East Adams Street, Syracuse, NY, 13210, 315-464-9950 (ph), 315-464-36638 (fax), oestm@upstate.edu.

The authors have no conflicts of interest to disclose.

retrievals and *in vivo* radiotherapy models are characterized by trabecular resorption, decreased cellularity, altered mineral density, and mesenchymal progenitor cell depletion.[2; 10–12]

Total body irradiation (animal) models consistently demonstrate trabecular bone loss and increased osteoclasts.[10; 13–15] In absence of osteolytic tumors, radiotherapy may be (somewhat counter-intuitively) associated with maintained or even increased bone mineral density in humans, suggesting anabolic osteoblast activity persists.[16–18] Using a focal hindlimb mouse irradiation (RTx) model, we demonstrated loss of metaphyseal trabeculae and decreased connectivity six weeks post-RTx (20 Gy), persisting through 26 weeks.[16] Cortical bone volume and mineral density were increased, suggesting that osteoblast activity continues post-RTx, but does not regenerate the osteoclast-resorbed trabecular bone.

Dose fractionation and beam targeting are currently the only clinical prophylaxes against radiation-associated skeletal morbidities. In order to develop effective preventative, diagnostic, and treatment strategies, we must first understand the post-radiotherapy course of biological events *in vivo*. Therefore, the goals of this study were to determine the time-dependent effects of focal irradiation on osteoclasts and mineral apposition rates using an established mouse model.

METHODS

Hindlimb Irradiation

Female BALB/F mice aged 12 weeks (Taconic, Germantown, NY) were anesthetized with one hindlimb extended for unilateral focal irradiation.[12; 16] All methods were approved by the SUNY Upstate Institutional Animal Care and Use Committee. Mice received a single (5 Gy) or four consecutive daily fractions (4x5 Gy) (n=6 mice/time point/group) using a 300kV beam at 10 mA. Additional mice were identically irradiated (4x5 Gy) for gene expression analysis (n=4/time point). Beam collimation and lead shielding sequestered the body and contralateral hindlimb from X-ray exposure (Philips RT-250, Andover, MA). The non-irradiated hindlimbs served as controls (0 Gy). Endpoints were 1, 2, 4, 8, 12, and 26 weeks after the last fraction of radiation was delivered.

Biologically effective doses (BEDs) were calculated to be 13.9 $Gy_{2.8}$ (5 Gy group) and 55.7 $Gy_{2.8}$ (4x5 Gy group).[19] The 4x5 Gy treatment group therefore delivered a $BED_{2.8}$ in the range of what is delivered clinically for the treatment of breast cancer metastases ($BED_{2.8}$=48.6–62.1 Gy, typical dose regime of 5x4 Gy or 10x3 Gy), but below that typically used in the treatment of chondrosarcomas (70–77.4 Gy using daily fractions of 1.8–2 Gy, $BED_{2.8}$=120–127 Gy) or myeloid sarcomas (6–35 Gy in 1.5–3.5 Gy fractions with a median or 20 Gy at 2 Gy/fraction, median $BED_{2.8}$=34.3).[20–22]

Histology

Mice received a calcein injection (10 mg/kg, sc) nine days before euthanasia to facilitate mineral apposition rate (MAR) measurements. Femurs were collected at 1, 2, 4, 8, 12, and 26 weeks post-RTx, then fixed (10% formalin, 4°C), and sequentially dehydrated (70%, 95%, 100% ethanol, xylene). Three-step methyl methacrylate (MMA) infiltration and

embedding was done under vacuum (59.3% MMA, 34.6% butyl methacrylate, 4.9% methyl benzoate, and 1.2% polyethylene glycol 400, with 0%, 0.4%, and then 0.8% benzoyl peroxide), all reagents from Sigma-Aldrich, St. Louis, MO). Embedded un-decalcified tissue was sectioned by microtome (5 μm thickness), mounted on (3-aminopropyl)triethoxysilane-coated slides, and stained for tartrate-resistant acid phosphatase (TRAP). MAR was determined from unstained tissue sections.

Imaging and Image Analysis

Micro-computed tomographic scans (μCT) of the distal femur were done for a representative subset of bones (n=3 per group per end point) (μCT 40, Scanco, Bassersdorf, Switzerland).[16] Reconstructed images were digitally segmented to illustrate trabecular and cortical morphologic changes (ImageJ, NIH, Bethesda, MD). Bone volume (BV) and bone mineral density (BMD) were quantified over the distal 5 mm of each femur, as was a 1 mm thick volume of cortical (BV) and 1 mm thick volume of trabecular bone (BV/TV) as previously described by Wernle et al.[16] Data were expressed as change relative to controls (Δ=[Experimental value] – [Average value for 0 Gy samples within that time point]).

Tissue sections were imaged in replicate at 40x magnification using a microscope (Nikon Eclipse E800M, Nikon, Melville, NY) equipped with a camera (SPOT Insight QE, Diagnostic Instruments, Sterling Heights, MI). Osteoclasts were enumerated over the distal 5 mm of each femur. Spatial distribution was assessed by dividing the imaged region into 13 axial bins and identifying the adherent surface: endosteal, periosteal, trabecular, and total.

Unstained tissue sections were imaged in duplicate by fluorescence microscopy at 40x, using a 488 nm filter (calcein label) and ultraviolet epifluorescence (bone). Corresponding images were digitally merged (Photoshop v12.0, Adobe, San Jose, CA) taken at 40x under fluorescence microscopy. After calibrating the linear measurement tool (ImageJ), the calcein label to bone margin distance was measured at the anterior and posterior aspects of four areas: endosteal and periosteal metaphysis (EM, PM), and endosteal and periosteal diaphysis (ED, PD) (Fig 5). Length measurements were normalized by calcein injection-to-euthanasia time, yielding mineral apposition rate (MAR, μm/day). Average (AVG) and total (∑) MAR were also calculated.

Gene Expression

Hindlimbs were collected at 1, 2, 4, 8, 12, and 26 weeks (4x5 Gy, n=4/time point). Femoral and tibial marrow was isolated and dissociated before RNA isolation (QiaShredder & RNeasy MiniPreps, Qiagen, Hilden, Germany) and transcription to cDNA (QuantiTect RT, Qiagen). Quantitative reverse transcription PCR (qRT-PCR) included ß-actin (reference), Runx2, bone-specific alkaline phosphatase (bsALP), cathepsin K, RANK ligand, and TRAP-5b genes (ep realplex2, Eppendorf, Hamburg, Germany). All reactions were run in duplicate (EvaGreen, Biotium, Hayward, CA) and product sizes verified electrophoretically. Relative expression (RE) was calculated using the Pfaffl method (E = primer efficiency, Ct = threshold cycle), where:[23]

$$RE = \frac{E_{\text{target}}^{(\Delta Ct_{\text{target}})}}{E_{\text{reference}}^{(\Delta Ct_{\text{reference}})}} \quad \text{and} \quad \Delta Ct = \left(Ct_{\text{experimental}} - Ct_{\text{control}}\right)$$

Statistics

Osteoclast number and MAR data were analyzed using a two-way ANOVA model with time, radiation dose, and their interaction (RTx*time) as independent variables (JMP software, SAS, Cary, NC). Post-hoc pairwise comparisons were conducted using Tukey's test. Statistical significance was defined at $p \leq 0.05$.

RESULTS

Radiation Induces Early Increases and Long-term Depletion of Osteoclasts

Radiation induced a biphasic osteoclast response (Table 1). Osteoclasts, located predominantly on metaphyseal trabecular surfaces (Fig 1), were increased at early time points but depleted long-term (Fig 2). Time was a significant variable for all regions (all $p \leq 0.003$), and RTx a significant variable for trabecular and total regions (both $p < 0.001$). The interaction term (RTx*time) was significant for the periosteal, trabecular, and total (all $p < 0.001$) regions.

One week post-RTx, trabecular and total osteoclasts were significantly increased in 5 Gy compared to both control and 4x5 Gy groups (all $p \leq 0.002$); the 4x5 Gy group did not differ from controls. Osteoclast numbers peaked at 2 weeks in both RTx groups, including significantly increased trabecular), periosteal, and total osteoclasts compared to controls (all $p \leq 0.003$). Osteoclasts decreased by week 4. RTx significantly depleted trabecular and total osteoclasts at 8, 12, and 26 weeks (all $p \leq 0.016$). Endosteal osteoclasts did not differ from controls at any time.

Bone Morphological Changes Correlate Temporally With Osteoclasts

RTx-induced trabecular resorption was apparent in μCT images (Fig 3).[16] In the 4x5 Gy group, trabecular bone loss was apparent 2–4 weeks post-RTx, persisting through week 26, while control bone trabeculae were maintained. Quantitative evaluation of morphologic bone changes indicated that bone volume (BV) and mineral density (BMD) in the distal femur were increased following RTx (Fig 4 A&B). Cortical thickening in the irradiated bones was pronounced by 2 weeks post-RTx, as determined by an increase in cortical bone volume over a 1mm thick volume of interest (Fig 4 C). Loss of metaphyseal trabecular bone (decreased BV/TV) was most pronounced in the 4x5 Gy group (Fig 4 D).

Mineral Apposition Rate Increases Transiently Following Irradiation

Mineral apposition occurred predominately at the endosteal metaphysis in all groups (Fig 5). Time was a significant variable; MAR decreased longitudinally in all groups (PD, ED, EM, AVG, and ∑ $p < 0.001$). Radiation was also a significant variable (PD, ED, EM, AVG, and ∑ all $p \leq 0.023$), as was their interaction term (RTx*time, EM, AVG, and ∑ $p < 0.001$). At 1 week, the 4x5 Gy group had increased ED, AVG, and ∑ MAR (all $p < 0.001$). MAR peaked

at 2 weeks in the 5 Gy group (ED, AVG, and ∑ $p<0.001$ vs. 0 Gy). The 4x5 Gy group demonstrated an unexpected spike in MAR at 8 weeks (ED, EM, AVG, and ∑ $p\leq0.009$ vs. 0 & 5 Gy).

Gene Expression

Runx2 expression increased (~2x) at 1 and 8 weeks post-RTx (Fig 6), while expression of bsALP increased slightly at 12 weeks. RANK-L, an osteoblast-secreted pro-osteoclastic factor, was upregulated (~2x) at weeks 2 and 8. Cathepsin K expression increased nearly 3x at 12 weeks, while TRAP-5b (tartrate-resistant acid phosphatase 5b) expression was elevated at 8 (~2x) and 26 weeks (~6x). Sample size (n=4) precluded statistical analysis.

DISCUSSION

The results from this study reveal that hindlimb radiation therapy to the distal femur induced an early increase in local osteoclast numbers, and this correlates temporally with extensive trabecular resorption. Early increased osteoclast numbers have also been demonstrated in total body irradiation models.[10; 13; 14] Trabecular bone lost due to early increased osteoclasts is not later restored. This aligns with established osteoblast behavior; matrix is preferentially deposited in apposition with existing bone or calcified cartilage. Following early RTx-induced osteoclastic trabecular resorption, osteoblasts have no scaffold to guide regeneration of trabeculae. Although murine epiphyses never completely close, the minimally active growth plates of our skeletally mature mice did not permit regeneration of fully resorbed trabeculae.

Following the early RTx-induced increase in osteoclast numbers, there is a persistent depletion of osteoclasts. The temporal variation in post-RTx osteoclast number (time, RTx, and their interaction were significant variables) suggests that responses to radiation may vary depending on the differentiation state of osteoclasts and their progenitor cells. The late-onset, long-term loss of osteoclasts may result from radiation-induced osteoclast progenitor death. Early after RTx, osteoclast numbers may be locally increased via recruitment of circulating precursors to the irradiated area, where they proceed to differentiate and resorb local bone. *In vivo*, osteoclast precursors can survive for an extended time in circulation.[24] However, primitive marrow-residing osteoclast progenitors are known to be highly radiosensitive, and their depletion could result in long-term loss of osteoclasts.[25; 26]

The late-onset, persistent loss of osteoclasts impairs homeostatic bone turnover and permits unopposed continuation of appositional matrix deposition. Morphologically, the result is increased cortical wall thickness. Persistent loss of osteoclasts and osteoclastic bone remodeling post-RTx may also increase bone fragility by permitting microdamage accumulation. Analogous to extended bisphosphonate therapy, mineralization without osteoclastic remodeling produces increasingly dense but embrittled matrix. In the absence of osteolytic tumors, post-radiotherapy fractures are not always associated with decreased bone mineral density clinically.[18; 19] Increased mineral density and cortical thickening are also present in animal radiotherapy models.[12; 16] Collectively, these data indicate continuation of mineral deposition post-RTx, but with compromised matrix quality.[27]

Mineral apposition rates did not, in general, increase post-RTx. However, MAR transiently increased at 1 and 8 weeks in 4x5 Gy samples, and 2 weeks in the 5 Gy group. The temporal variation in osteoclasts and MAR between the 5 Gy and 4x5 Gy groups at 1 and 2 weeks is likely a timing artifact; irradiation of 5 Gy samples coincided with the first fraction for the 4x5 Gy group; the one-week time point occurred 7 days after fourth fraction. O'Donovan et al. reported increased osteoblasts and continued appositional mineral deposition 14 weeks post-RTx (35 Gy) in a rabbit mandibular model.[28] Our data similarly demonstrate increased MAR and Runx2 expression 8 weeks post-RTx, suggesting a delayed and transient increase in osteoblastic differentiation and activity. Mesenchymal stem cells (MSCs) are radiosensitive, but capable of self-replenishing and restoring the marrow niche.[29; 30] The delayed MAR increase (8 weeks in our 4x5 Gy samples) may be a result of MSCs repopulating the marrow niche before renewing osteoblasts. Existing osteoblast activity, including bsALP activity and Runx2 expression, may however be upregulated post-RTx.[29] Increased activity of existing osteoblasts may explain the 1 week post-RTx increase in Runx2 expression and MAR.

Using *in vitro* models, others have demonstrated transient RTx suppression of osteoblastic MSC differentiation, including Runx2 expression and delayed cell cycling.[31; 32] The more robust osteoblast progenitors may survive RTx in greater numbers than osteoclast progenitors.[33] Transient RTx-induced osteoblast progenitor suppression may contribute to the delayed MAR increase in the 4x5 Gy group here. This hypothesis is supported by the temporal correlation of MAR and Runx2 expression at 8 weeks, as Runx2 is involved in osteoblastic MSC differentiation.

Osteoblasts and their precursors can promote osteoclastic differentiation and proliferation in response to radiation through increased RANKL and MCSF production.[34] Radiation can directly activate osteoclast progenitors via upregulation of RANK, integrin ß3, and TRAP.[35] Here, the increased RANKL production at 2 weeks post-RTx suggests that early increased osteoclast numbers may result from both direct and osteoblast-mediated activation of osteoclasts. The increase in cathepsin K and TRAP5b gene expression at 12 and 26 weeks, respectively, does not obviously correlate with the late depletion of osteoclasts documented histologically. This is potentially a sampling error – qRT-PCR was run using marrow lysate from the entire femur, while osteoclasts and MAR were quantified only over the distal femur which was more directly in the field of radiation.

The incidence of fragility fractures in non-osteopenic RTx patients suggests bone quality contributes to fracture risk. Physiochemical changes in bone quality, including accumulation of fragmented or pathologically cross-linked collagen and abnormal hydroxyapatite crystals, can be initiated by radiation and contribute to bone fragility.[27; 36; 37] In animal models, irradiated bone loses mechanical strength and can become embrittled, despite increased mineral density.[16] The nature of these changes makes predicting radiation-associated fragility fractures in non-osteopenic patients difficult. Clinical methods for assessing osteoporotic fracture risk rely on densitometry, which is unable to detect the changes in bone quality characteristic of radiation-associated fracture risk.

This study is, to our knowledge, the first to illustrate persistent, long-term loss of osteoclasts following radiotherapy. In the absence of osteoclastic remodeling, appositional bone growth continues unopposed and leads to increased bone mineral density, cortical thickening, decreased remodeling, and accumulation of poor quality matrix. Trabecular bone lost to early increased osteoclast activity is not later restored, suggesting that early attenuation of osteoclasts may prevent local trabecular bone loss in radiotherapy patients, possibly preserving bone strength. We have previously demonstrated attenuation of post-RTx (1x20 Gy) trabecular bone resorption by zoledronate treatment in mice.[12; 38]

There are multiple mechanisms by which radiation therapy contributes to bone fragility and increased fracture risk, including 1) activation of existing osteoclasts; 2) loss of osteoclast progenitors; 3) decreased bone turnover; 4) compromised matrix and material properties; and 5) loss of trabecular bone.[33] The biphasic changes in osteoclast numbers suggest that while antiresorptive therapies could protect existing bone from resorption, the unopposed mineral apposition and accumulation of microdamage resulting from long-term loss of osteoclasts would remain unaddressed. Further work is needed to identify the specific contributions of these multiple mechanisms to bone fragility, their regulatory mechanisms, and to develop appropriate preventative, diagnostic, and therapeutic tools for clinical use.

ACKNOWLEDGEMENTS

This study was funded by the Carol M. Baldwin Breast Cancer Research Foundation (MEO), Kate Allen Breast Cancer Research Fund (TAD), David G. Murray Endowment (TAD), and NIH/NIAMS Award AR065419 (TAD).

REFERENCES

1. Baxter NN, Habermann EB, Tepper JE, et al. Risk of pelvic fractures in older women following pelvic irradiation. JAMA. 2005; 294:2587–2593. [PubMed: 16304072]
2. Guise TA. Bone loss and fracture risk associated with cancer therapy. Oncologist. 2006; 11:1121–1131. [PubMed: 17110632]
3. Oh D, Huh SJ, Nam H, et al. Pelvic insufficiency fracture after pelvic radiotherapy for cervical cancer: analysis of risk factors. Int J Radiat Oncol Biol Phys. 2008; 70:1183–1188. [PubMed: 17919836]
4. Oster G, Lamerato L, Glass AG, et al. Natural history of skeletal-related events in patients with breast, lung, or prostate cancer and metastases to bone: a 15-year study in two large US health systems. Support Care Cancer. 2013; 21:3279–3286. [PubMed: 23884473]
5. Park SH, Kim JC, Lee JE, et al. Pelvic insufficiency fracture after radiotherapy in patients with cervical cancer in the era of PET/CT. Radiat Oncol J. 2011; 29:269–276. [PubMed: 22984680]
6. Dunlap NE, Cai J, Biedermann GB, et al. Chest wall volume receiving >30 Gy predicts risk of severe pain and/or rib fracture after lung stereotactic body radiotherapy. Int J Radiat Oncol. Biol Phys. 2010; 76:796–801. [PubMed: 19427740]
7. Voroney JP, Hope A, Dahele MR, et al. Chest wall pain and rib fracture after stereotactic radiotherapy for peripheral non-small cell lung cancer. J Thorac Oncol. 2009; 4:1035–1037. [PubMed: 19633478]
8. Helmstedter CS, Goebel M, Zlotecki R, et al. Pathologic fractures after surgery and radiation for soft tissue tumors. Clin Orthop Relat Res:. 2001:165–172. [PubMed: 11501806]
9. Holt GE, Griffin AM, Pintilie M, et al. Fractures following radiotherapy and limb-salvage surgery for lower extremity soft-tissue sarcomas. A comparison of high-dose and low-dose radiotherapy. J Bone Joint Surg Am. 2005; 87:315–319. [PubMed: 15687153]
10. Bandstra ER, Pecaut MJ, Anderson ER, et al. Long-term dose response of trabecular bone in mice to proton radiation. Radiat Res. 2008; 169:607–614. [PubMed: 18494551]

11. Green DE, Adler BJ, Chan ME, et al. Devastation of adult stem cell pools by irradiation precedes collapse of trabecular bone quality and quantity. J Bone Miner Res. 2012; 27:749–759. [PubMed: 22190044]
12. Keenawinna L, Oest ME, Mann KA, et al. Zoledronic acid prevents loss of trabecular bone after focal irradiation in mice. Radiat Res. 2013; 180:89–99. [PubMed: 23772924]
13. Willey JS, Livingston EW, Robbins ME, et al. Risedronate prevents early radiation-induced osteoporosis in mice at multiple skeletal locations. Bone. 2010; 46:101–111. [PubMed: 19747571]
14. Willey JS, Lloyd SA, Robbins ME, et al. Early increase in osteoclast number in mice after whole-body irradiation with 2 Gy X rays. Radiat Res. 2008; 170:388–392. [PubMed: 18763868]
15. Hamilton SA, Pecaut MJ, Gridley DS, et al. A murine model for bone loss from therapeutic and space-relevant sources of radiation. J Appl Physiol. 2006; 101:789–793. [PubMed: 16741258]
16. Wernle JD, Damron TA, Allen MJ, et al. Local irradiation alters bone morphology and increases bone fragility in a mouse model. J Biomech. 2010; 43:2738–2746. [PubMed: 20655052]
17. Damron TA. CORR Insights: Do Long Term Survivors of Ewing Family of Tumors Experience Low Bone Mineral Density and Increased Fracture Risk? Clin Orthop Relat Res. 2014
18. Dhakal S, Chen J, McCance S, et al. Bone density changes after radiation for extremity sarcomas: exploring the etiology of pathologic fractures. Int J Radiat Oncol Biol Phys. 2011; 80:1158–1163. [PubMed: 20888134]
19. Hopewell JW. Radiation-therapy effects on bone density. Med Pediatr Oncol. 2003; 41:208–211. [PubMed: 12868120]
20. Rordorf T, Hassan AA, Azim H, et al. Bone health in breast cancer patients: A comprehensive statement by CECOG/SAKK Intergroup. Breast. 2014
21. Patel S, DeLaney TF. Advanced-technology radiation therapy for bone sarcomas. Cancer Control. 2008; 15:21–37. [PubMed: 18094658]
22. Chen WY, Wang CW, Chang CH, et al. Clinicopathologic features and responses to radiotherapy of myeloid sarcoma. Radiat Oncol. 2013; 8:245. [PubMed: 24148102]
23. Pfaffl, MW. Quantification Strategies in real-time PCR. In: Bustin, SA., editor. A-Z of quantitative PCR. La Jolla CA: International University Line; 2004. p. 87-112.
24. Turner RT, Evans GL, Wakley GK. Reduced chondroclast differentiation results in increased cancellous bone volume in estrogen-treated growing rats. Endocrinology. 1994; 134:461–466. [PubMed: 7506213]
25. Scheven BA, Wassenaar AM, Kawilarang-de Haas EW, et al. Comparison of direct and indirect radiation effects on osteoclast formation from progenitor cells derived from different hemopoietic sources. Radiat Res. 1987; 111:107–118. [PubMed: 3602348]
26. Hirabayashi Y. Radiation-induced, cell cycle-related gene expression in aging hematopoietic stem cells: enigma of their recovery. Ann N Y Acad Sci. 2014; 1310:69–73. [PubMed: 24611895]
27. Gong B, Oest ME, Mann KA, et al. Raman spectroscopy demonstrates prolonged alteration of bone chemical composition following extremity localized irradiation. Bone. 2013; 57:252–258. [PubMed: 23978492]
28. O'Donovan DA, La Scala GC, Leong I, et al. Radiation-induced craniofacial bone growth inhibition: acute and long-term effects on bone histopathology with and without cytoprotection. Plast Reconstr Surg. 2012; 129:636e–645e.
29. Poncin G, Beaulieu A, Humblet C, et al. Characterization of spontaneous bone marrow recovery after sublethal total body irradiation: importance of the osteoblastic/adipocytic balance. PLoS One. 2012; 7:e30818. [PubMed: 22363493]
30. Ma J, Shi M, Li J, et al. Senescence-unrelated impediment of osteogenesis from Flk1+ bone marrow mesenchymal stem cells induced by total body irradiation and its contribution to long-term bone and hematopoietic injury. Haematologica. 2007; 92:889–896. [PubMed: 17606438]
31. Sakurai T, Ito M, Mikamoto T, et al. Ionising irradiation-induced inhibition of differentiation of C3H10T1/2 cells to the osteoblastic lineage. Int J Radiat Biol. 2011; 87:447–452. [PubMed: 21219113]
32. Park SS, Kim KA, Lee SY, et al. X-ray radiation at low doses stimulates differentiation and mineralization of mouse calvarial osteoblasts. BMB Rep. 2012; 45:571–576. [PubMed: 23101511]

33. Green DE, Rubin CT. Consequences of irradiation on bone and marrow phenotypes, and its relation to disruption of hematopoietic precursors. Bone. 2014; 63C:87–94. [PubMed: 24607941]

34. Yang B, Tang Q, Post J, et al. Effect of radiation on the Notch signaling pathway in osteoblasts. Int J Mol Med. 2013; 31:698–706. [PubMed: 23340672]

35. Yang B, Zhou H, Zhang XD, et al. Effect of radiation on the expression of osteoclast marker genes in RAW264.7 cells. Mol Med Rep. 2012; 5:955–958. [PubMed: 22294242]

36. Oest ME, Damron TA. Focal Therapeutic Irradiation Induces an Early Transient Increase in Bone Glycation. Radiat Res. 2014

37. Green DE, Adler BJ, Chan ME, et al. Altered composition of bone as triggered by irradiation facilitates the rapid erosion of the matrix by both cellular and physicochemical processes. PLoS One. 2013; 8:e64952. [PubMed: 23741433]

38. Arrington SA, Damron TA, Mann KA, et al. Concurrent administration of zoledronic acid and irradiation leads to improved bone density, biomechanical strength, and microarchitecture in a mouse model of tumor-induced osteolysis. J Surg Oncol. 2008; 97:284–290. [PubMed: 18161868]

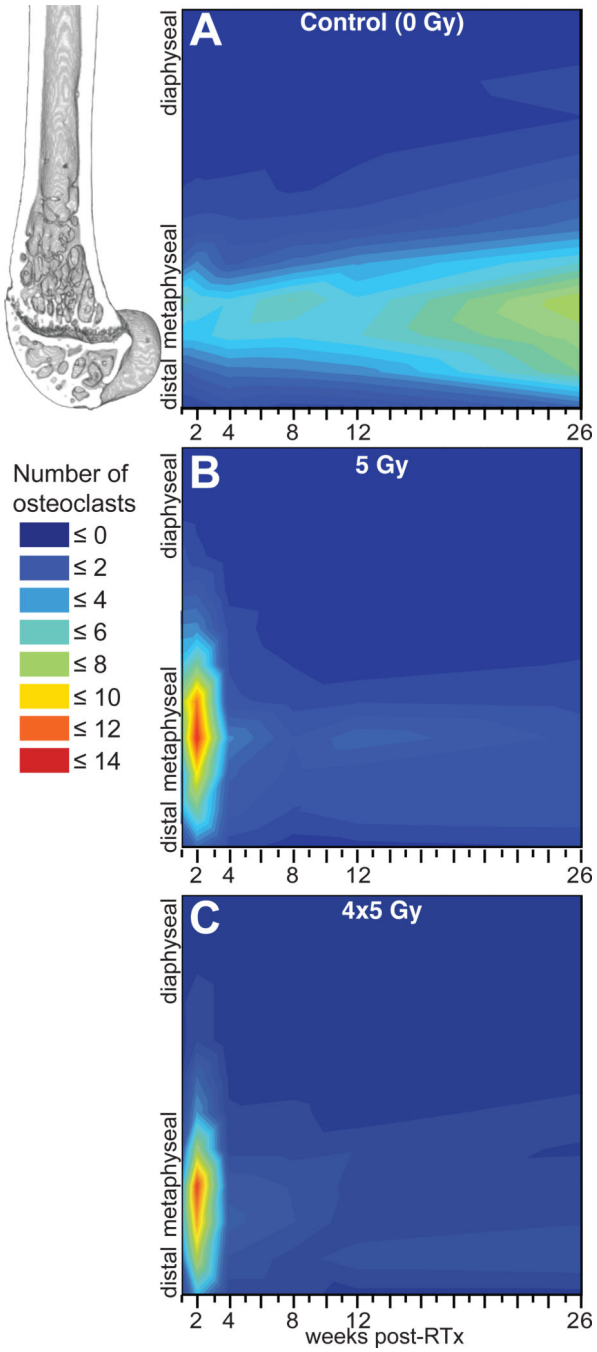

Figure 1.

Temporal (abscissa) and longitudinal (ordinate) distribution of osteoclasts in the distal femur for hindlimbs irradiated with 0 Gy (A), 5 Gy (B), and 4x5 Gy (C).

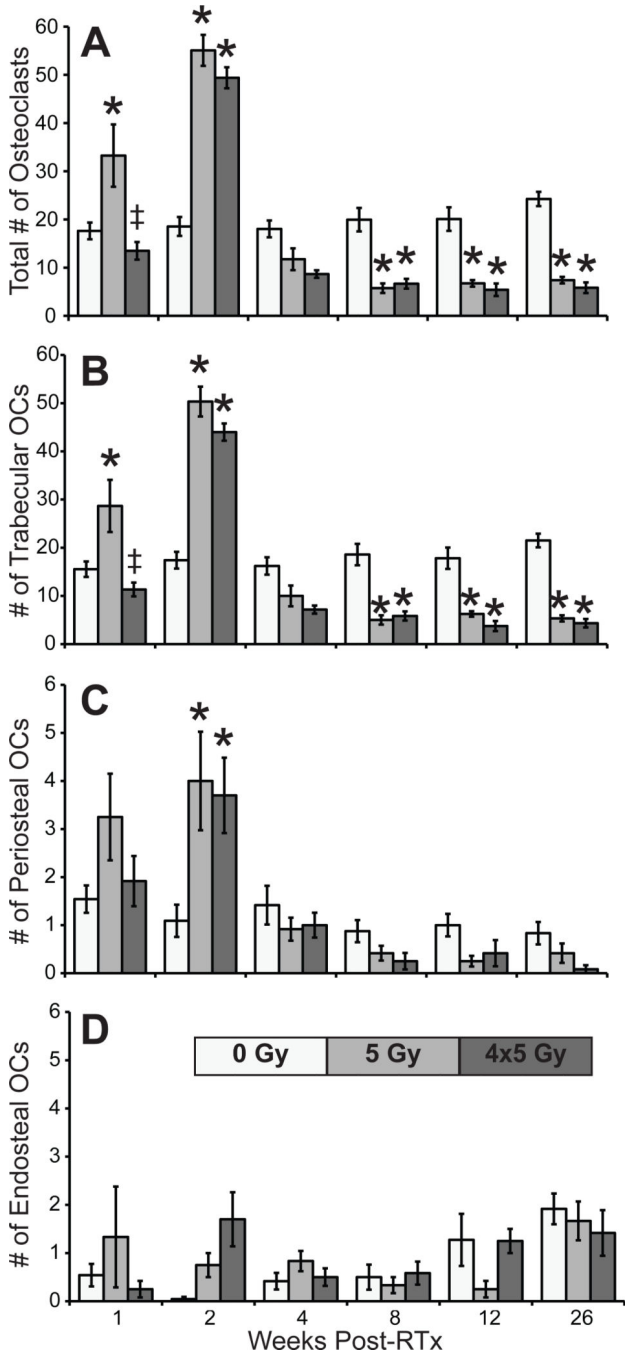

Figure 2.

Number of osteoclasts in the distal 5mm of the femurs (A), and on the distal femoral trabecular (B), periosteal (C), and endosteal (D) surfaces (average ±SEM; *p<0.05 vs. 0 Gy).

Figure 3.

Representative μCT images from 0 Gy, 5 Gy, and 4x5 Gy distal femurs. Upper rows: sagittal sections (digitally bisected). Lower rows: corresponding transverse metaphyseal sections.

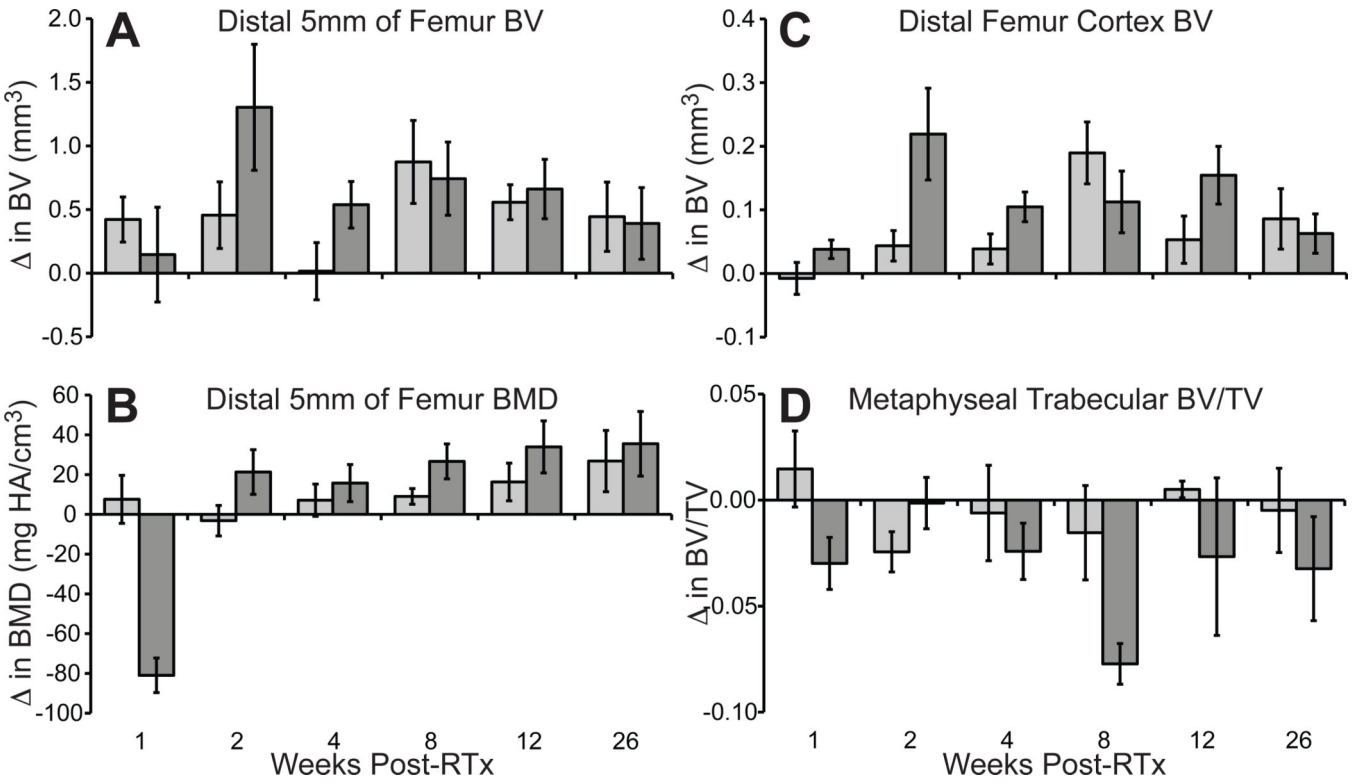

Figure 4.

Micro-CT quantification of morphologic bone changes, expressed as change relative to non-irradiated control limbs (experimental - average value of 0 Gy limbs) +/− SEM (n=2–6 per time point). Over the distal 5mm of the femur, bone volume (A) was increased following irradiation, and bone mineral density (B) also increased following a brief, transient decrease at 1 week in the 5 Gy group. Radiation-induced cortical thickening was demonstrated by an increase in the BV (C) over a 1mm thick distal femur volume of interest. Loss of trabecular bone (D) was most pronounced in the 4x5 Gy group.

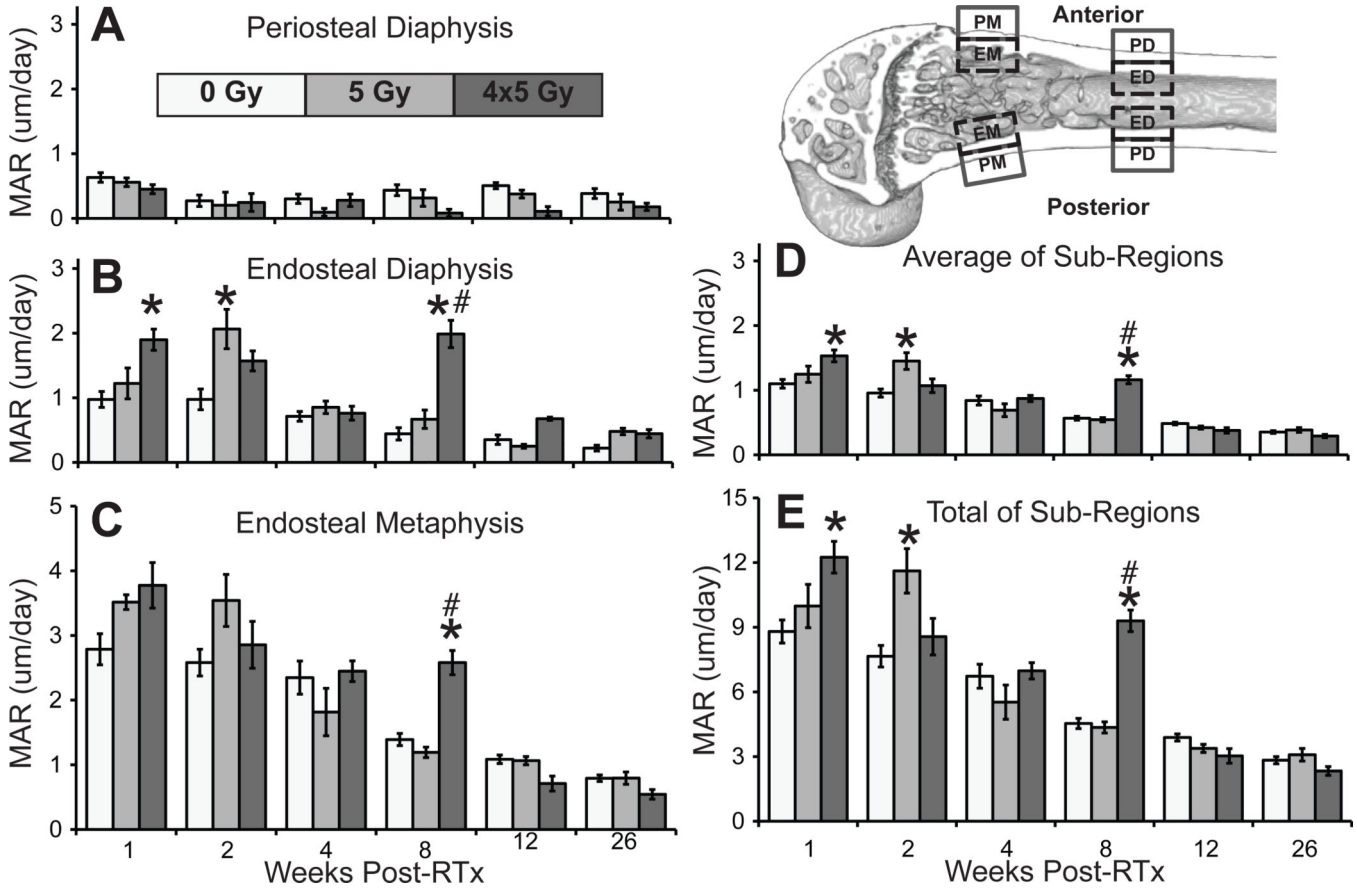

Figure 5.

Mineral apposition rates at the periosteal (A) and endosteal diaphysis (B), and endosteal metaphysis (C), including average (D) and total (E) MAR. Periosteal metaphyseal contribution was ≤0.67% of ∑ (average ±SEM; *p<0.05 vs. 0 Gy; #p<0.05 vs. 5 Gy). Top left: regions of interest used in mineral apposition rate (MAR) analysis: endosteal metaphysis (EM), periosteal metaphysis (PM), endosteal diaphysis (ED), and periosteal diaphysis (PD) surfaces at both the anterior and posterior aspects of the distal femur.

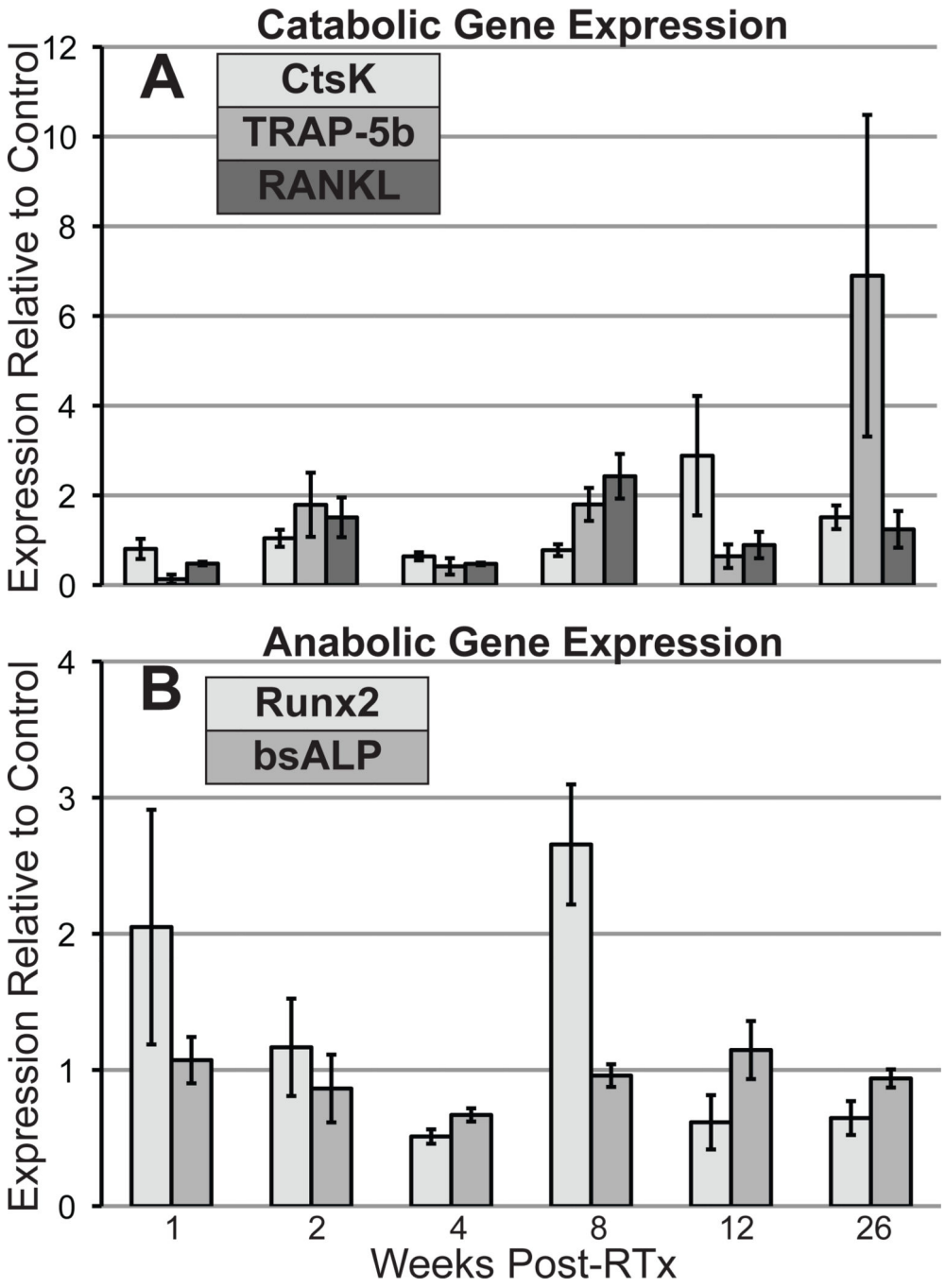

Figure 6.

Quantitative reverse-transcription PCR analysis of catabolic (A) and anabolic (B) gene expression in the bone marrow, shown as expression relative to control limbs (average ±SEM).

Table 1

Osteoclast numbers and mineral apposition rates in the distal femur following irradiation.

Treatment (Gy)	Time (weeks)	Sample Size	Number of Osteoclasts (#)				Mineral Apposition Rate (um/day)					
			Trabecular	Periosteal	Endosteal	Distal 5mm	Periosteal Diaphysis	Endosteal Diaphysis	Periosteal Metaphysis	Endosteal Metaphysis	Average	Total
0 Gy	1	n = 12	15.5 ± 1.6	1.5 ± 0.3	0.5 ± 0.2	17.6 ± 1.7	0.63 ± 0.26	0.98 ± 0.42	0.01 ± 0.02	2.79 ± 0.83	1.10 ± 0.23	8.80 ± 1.85
	2	n = 11	17.4 ± 1.7	1.1 ± 0.3	0.0 ± 0.0	18.5 ± 2.0	0.27 ± 0.29	0.98 ± 0.53	0.00 ± 0.00	2.58 ± 0.68	0.96 ± 0.21	7.65 ± 1.66
	4	n = 12	16.2 ± 1.8	1.4 ± 0.4	0.4 ± 0.2	18.0 ± 1.7	0.30 ± 0.25	0.71 ± 0.26	0.00 ± 0.00	2.35 ± 0.89	0.84 ± 0.24	6.73 ± 1.93
	8	n = 12	18.6 ± 2.2	0.9 ± 0.2	0.5 ± 0.3	20.0 ± 2.4	0.43 ± 0.29	0.44 ± 0.33	0.00 ± 0.00	1.39 ± 0.33	0.57 ± 0.10	4.54 ± 0.82
	12	n = 11	17.8 ± 2.2	1.0 ± 0.2	1.3 ± 0.5	20.1 ± 2.4	0.51 ± 0.16	0.35 ± 0.25	0.00 ± 0.00	1.09 ± 0.23	0.49 ± 0.07	3.89 ± 0.56
	26	n = 12	21.5 ± 1.4	0.8 ± 0.2	1.9 ± 0.3	24.3 ± 1.5	0.38 ± 0.27	0.22 ± 0.16	0.02 ± 0.07	0.79 ± 0.17	0.35 ± 0.07	2.83 ± 0.58
5 Gy	1	n = 6	*28.7 ± 5.4	3.3 ± 0.9	1.3 ± 1.0	*33.3 ± 6.5	0.56 ± 0.17	1.22 ± 0.59	0.02 ± 0.04	3.51 ± 0.28	1.25 ± 0.31	9.98 ± 2.46
	2	n = 6	*50.3 ± 3.1	*4.0 ± 1.0	0.8 ± 0.3	*55.1 ± 3.2	0.20 ± 0.49	*2.06 ± 0.75	0.00 ± 0.00	3.54 ± 0.98	*1.45 ± 0.32	11.61 ± 2.52
	4	n = 6	10.0 ± 2.2	0.9 ± 0.2	0.8 ± 0.2	11.8 ± 2.3	0.09 ± 0.15	0.85 ± 0.24	0.00 ± 0.00	1.82 ± 0.90	0.69 ± 0.24	5.53 ± 1.95
	8	n = 6	*5.0 ± 1.0	0.4 ± 0.2	0.3 ± 0.2	*5.8 ± 1.0	0.31 ± 0.31	0.67 ± 0.35	0.00 ± 0.00	1.19 ± 0.20	0.54 ± 0.08	4.35 ± 0.63
	12	n = 6	*6.3 ± 0.6	0.3 ± 0.1	0.3 ± 0.2	*6.8 ± 0.7	0.38 ± 0.15	0.25 ± 0.07	0.00 ± 0.00	1.06 ± 0.16	0.42 ± 0.06	3.38 ± 0.46
	26	n = 6	*5.3 ± 0.6	0.4 ± 0.2	1.7 ± 0.4	*7.4 ± 0.7	0.25 ± 0.31	0.48 ± 0.12	0.02 ± 0.04	0.79 ± 0.23	0.39 ± 0.09	3.08 ± 0.72
4x5 Gy	1	n = 6	#11.3 ± 1.4	1.9 ± 0.5	0.3 ± 0.2	#13.5 ± 1.8	0.45 ± 0.17	*1.90 ± 0.40	0.00 ± 0.00	3.78 ± 0.86	*1.53 ± 0.22	*12.25 ± 1.80
	2	n = 5	*44.0 ± 1.8	*3.7 ± 0.8	1.7 ± 0.6	*49.4 ± 2.2	0.24 ± 0.31	1.57 ± 0.34	0.00 ± 0.00	2.86 ± 0.81	1.07 ± 0.24	8.56 ± 1.90
	4	n = 6	7.2 ± 0.8	1.0 ± 0.3	0.5 ± 0.2	8.7 ± 0.8	0.28 ± 0.23	0.76 ± 0.26	0.00 ± 0.00	2.45 ± 0.39	0.87 ± 0.12	6.98 ± 0.93
	8	n = 6	*5.8 ± 1.0	0.3 ± 0.2	0.6 ± 0.2	*6.7 ± 1.0	0.08 ± 0.14	*#1.99 ± 0.52	0.00 ± 0.00	*#2.58 ± 0.46	*#1.16 ± 0.15	*#9.30 ± 1.23
	12	n = 6	*3.8 ± 1.0	0.4 ± 0.3	1.3 ± 0.3	*5.4 ± 1.3	0.11 ± 0.18	0.68 ± 0.06	0.02 ± 0.05	0.71 ± 0.28	0.38 ± 0.10	3.03 ± 0.82
	26	n = 6	*4.3 ± 0.9	0.1 ± 0.1	1.4 ± 0.5	*5.8 ± 1.1	0.18 ± 0.14	0.45 ± 0.16	0.00 ± 0.00	0.54 ± 0.18	0.29 ± 0.06	2.33 ± 0.50

Osteoclast numbers and mineral apposition rates (MARs, average ± SEM;

*p<0.05 vs. 0 Gy;

#p<0.05 vs. 5 Gy).